Greensphere:
Journal of Environmental Chemistry
ISSN: 2777-0664
Original Article

Study of MnO_2/Ni-MCM-41 Catalyst for CO Oxidation in Motorcycle Exhaust Emissions

Alvin Romadhoni Putra Hidayat[1*], Alvin Rahmad Widyanto[2], Ratna Ediati[3], Hafildatur Rosyidah[3], Romario Abdullah[4]

[1] Department of Chemistry, Diponegoro University, Semarang 50275, Indonesia
[2]Department of Applied Chemistry, Shibaura Institute of Technology, 3-7-5 Toyosu, Koto-ku, Tokyo 135-8548, Japan
[3] Department of Chemistry, Institut Teknologi Sepuluh Nopember, Surabaya 60111, Indonesia
[4]College of Vocational Studies, Bogor Agricultural University (IPB University), Bogor, Indonesia

**Corresponding author*: alvinromadhoniputrah@lecturer.undip.ac.id

Received: 17 April 2026 / Accepted: 28 Mei 2026
Available online: 31 Mei 2026

Abstract

Incomplete combustion in vehicles produces hazardous gases such as carbon monoxide (CO), which is harmful to human health. This study aimed to synthesize MnO_2/Ni-MCM-41 as a catalyst for CO oxidation to CO_2. MCM-41 was synthesized via a hydrothermal method, followed by Ni doping to form Ni-MCM-41 and subsequent wet impregnation to obtain MnO_2/Ni-MCM-41. The materials were characterized by FTIR, XRD, TEM, and N_2 physisorption, while catalytic activity for CO oxidation was evaluated using a four-stroke motorcycle. FTIR spectra showed a band at 1633.76 cm^{-1} attributed to –OH vibrations corresponding to Si–OH groups in MCM-41, whereas XRD patterns exhibited characteristic peaks at $2\theta = 2.5°$ for MCM-41 and $2\theta = 25°$ for δ-MnO_2. TEM analysis confirmed the hexagonal mesostructure of MCM-41, consistent with previous reports, while N_2 physisorption revealed a type IV isotherm, indicating a mesoporous structure. Ni incorporation decreased the specific surface area but may promote catalytic activity through improved oxygen mobility and enhanced interaction between Mn species and the mesoporous support. Increasing reaction time reduced CO concentration, while CO_2 concentration increased correspondingly, confirming effective catalytic oxidation activity. The optimum catalytic performance was obtained for MnO_2/Ni-MCM-41 with an impregnation time of 10 h under real motorcycle exhaust conditions.

Keywords: *CO Oxidation, Catalyst, Ni-MCM-41, Catalytic Converter, MnO_2*

1. Introduction

Human mobility has increased significantly along with urbanization and economic development, resulting in the continuous growth of motorized transportation. In Indonesia, motorcycles dominate daily mobility because they are affordable, flexible, and practical for urban travel. However, this high dependence on motorcycles contributes to the deterioration of urban air quality. Road transportation has been identified as an important source of energy consumption and emissions in Indonesian cities [1]. Real-world emission measurements in Jakarta also indicate that motor vehicles, including motorcycles, remain a major contributor to urban air pollutants [2]. Motorcycle exhaust emissions commonly contain harmful pollutants such as carbon monoxide (CO), hydrocarbons (HC), and nitrogen oxides (NOx), which are mainly produced from incomplete combustion in internal combustion engines [3]–[5].

Among these pollutants, CO is considered highly hazardous because it is colorless, odorless, and toxic. CO can bind strongly to hemoglobin, reduce oxygen transport in the blood, and cause tissue hypoxia, which may lead to severe health effects at high exposure levels [6], [7]. Therefore, emission control technologies are needed to reduce CO concentration in vehicle exhaust gases. Catalytic oxidation is one of the most effective approaches for converting CO into CO_2. Manganese oxide catalysts have attracted attention for CO oxidation because Mn species can exist in multiple oxidation states and provide active oxygen species during the reaction [8]–[10]. However, bulk metal oxide catalysts often show

limited performance due to low surface area, poor active-site dispersion, and mass transfer limitations.

Mesoporous silica materials such as MCM-41 are widely used as catalyst supports because they have ordered pore structures, high surface area, and good chemical stability. These characteristics can improve the dispersion of active species and facilitate molecular diffusion in the pore system [11], [12]. Modification of MCM-41 with transition metals such as nickel can further enhance catalytic properties by introducing additional active sites and improving metal-support interaction [13], [14]. Based on these considerations, the combination of MnO_2 and Ni-modified MCM-41 is expected to improve catalytic activity for CO oxidation. MnO_2 provides redox-active sites, while Ni-MCM-41 supports active-site dispersion, gas diffusion, and oxygen mobility. Therefore, this study aims to develop MnO_2/Ni-MCM-41 as a catalytic system for reducing CO emissions from motorcycle exhaust gases.

2. Experimental Section

2.1 Chemicals and Instrumentation

The materials used in this study were sodium metasilicate nonahydrate ($Na_2SiO_3 \cdot 9H_2O$, Merck) as the silica precursor, cetyltrimethylammonium bromide (CTABr, >99%, Merck) as the structure-directing agent, sodium hydroxide (NaOH, Carlo Erba), sulfuric acid (H_2SO_4, 96%, Merck), nickel chloride, manganese sulfate ($MnSO_4$), demineralized water, ethanol, and universal pH paper. These chemicals were used without further purification. The synthesized materials were characterized using X-ray diffraction (XRD), Fourier transform infrared spectroscopy (FTIR), transmission electron microscopy (TEM), and N_2 adsorption-desorption analysis with the Brunauer-Emmett-Teller (BET) method. These techniques are commonly applied to evaluate the crystallographic structure, functional groups, morphology, and textural properties of mesoporous silica-based catalysts [15], [16].

2.2 Experimental Methods

2.2.1 Ni-MCM-41 Synthesis

Ni-MCM-41 was synthesized using a hydrothermal method with a Si/Ni molar ratio of 15. Hydrothermal synthesis is commonly used for preparing MCM-41 and metal-modified MCM-41 because it supports the formation of ordered mesoporous silica structures in the presence of a surfactant template [15], [17]. Sodium metasilicate (12.7077 g, 0.1 mol) was dissolved in 50 mL of demineralized water and stirred at 300 rpm for 15 min. Separately, 1.6070 g of nickel chloride and 9.1006 g of CTABr were dissolved in 50 mL and 80 mL of demineralized water, respectively, and stirred for 15 min.

The sodium metasilicate solution was slowly added to the CTABr solution under continuous stirring and then stirred for 30 min. The nickel chloride solution was added afterward, followed by additional stirring for 30 min until a gel was formed. The molar composition of the gel was 0.1 SiO_2 / 0.0067 $NiCl_2$ / 0.025 CTABr / 10 H_2O. The pH of the gel was adjusted to 10.5–11 using 4 N H_2SO_4 until a suspension was obtained. The suspension was aged in an oven at 100 °C for 144 h. After cooling, the solid product was filtered and washed with demineralized water until neutral pH was reached. The product was then dried at 100 °C for 12 h, ground, and calcined at 550 °C for 6 h to remove the organic template and obtain Ni-MCM-41. Calcination after hydrothermal synthesis is important to remove the surfactant template and open the mesoporous channel system [16], [17].

2.2.2 Impregnation of Ni-MCM-41 with $MnSO_4$

MnO_2 loading was carried out using the wet impregnation method with $MnSO_4$ as the manganese precursor. Wet impregnation is widely used to introduce metal oxide species into mesoporous supports because the precursor solution can enter the pore system and deposit active species after drying and calcination [16], [18]. In this study, 0.5 g of Ni-MCM-41 was dispersed in 1 M $MnSO_4$ solution and stirred for 5, 10, and 15 h. The impregnated samples were dried at 100 °C and then calcined at 550 °C to obtain MnO_2/Ni-MCM-41 catalysts.

2.2.3 Material Characterization

Ni-MCM-41 was characterized using XRD, TEM, and N_2 adsorption-desorption analysis. XRD was used to identify the ordered mesoporous structure and diffraction pattern of the synthesized material. TEM was used to observe the morphology and mesostructural arrangement of Ni-MCM-41. N_2 adsorption-desorption analysis was used to determine the specific surface area, pore volume, and pore diameter of the material. The BET method is commonly used to calculate the specific surface area of porous materials, while pore structure analysis is used to evaluate mesoporosity and possible pore blockage after metal incorporation [16], [19].

MnO_2/Ni-MCM-41 catalysts were characterized using XRD and FTIR. XRD analysis was conducted to identify structural changes and crystalline phases after MnO_2 impregnation. FTIR analysis was used to identify functional groups and metal-oxygen vibrations present in the catalyst. The presence of Si-O-Si, Si-OH, Si-O-Ni, and Mn-O vibrations can provide evidence of silica framework formation, nickel modification, and manganese oxide incorporation in the mesoporous support [15], [16], [18].

2.2.4 Catalytic Activity Test for CO Oxidation

Catalytic activity was evaluated using exhaust gas from a four-stroke motorcycle under idle conditions. Three catalyst conditions were tested: without catalyst, MnO_2, and MnO_2/Ni-MCM-41 with different impregnation times. Approximately 0.5 g of catalyst was placed on a Cu plate positioned in the exhaust stream. CO and CO_2 concentrations were measured using an E-COM gas analyzer. Each test was repeated three times under identical conditions to improve data reliability. The catalytic performance

was evaluated based on CO conversion using the following equation:

$$\text{CO Conversion (\%)} = \frac{[CO]_{in} - [CO]_{out}}{[CO]_{in}} \times 100$$

where $[CO]_{in}$represents the initial CO concentration before contact with the catalyst and $[CO]_{out}$ represents the CO concentration after contact with the catalyst. CO_2 formation was also observed to evaluate the oxidation of CO into CO_2. This approach is consistent with catalytic CO oxidation studies, where a decrease in CO concentration and an increase in CO_2 concentration indicate oxidation activity over the catalyst surface [8]–[10].

3. Results and Discussion

3.1 Synthesis and Characterization of Ni-MCM-41

3.1.1 XRD Analysis

The synthesized Ni-MCM-41 was first analyzed using XRD to confirm the formation of the mesoporous structure. The XRD pattern showed a strong diffraction peak at 2θ ≈ 2.5° and two weak peaks in the range of 2θ = 3.5–6.7°, , as shown in Fig. 1. These peaks are characteristic of MCM-41-type mesoporous silica with an ordered hexagonal structure. Similar diffraction characteristics have been reported for metal-modified MCM-41, where low-angle diffraction peaks indicate the presence of an ordered mesoporous framework [15], [17]. The appearance of these peaks indicates that the hydrothermal synthesis successfully produced Ni-MCM-41 while maintaining the ordered silica structure.

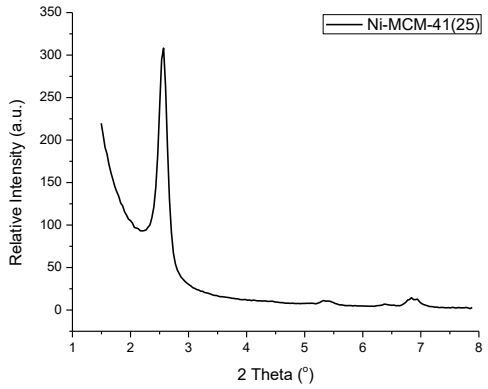

Fig. 1. Diffractogram pattern of Ni-MCM-41

3.1.2 TEM Analysis

TEM analysis was carried out to observe the morphology and pore arrangement of the synthesized Ni-MCM-41. The TEM image showed an ordered mesoporous structure, as shown in Fig. 2, which indicates that the material retained the typical hexagonal arrangement of MCM-41. This result supports the XRD analysis and shows that nickel modification did not significantly damage the mesoporous framework. Previous studies also reported that MCM-41 and metal-modified MCM-41 can maintain their ordered mesostructure when synthesized under controlled hydrothermal conditions [15], [17].

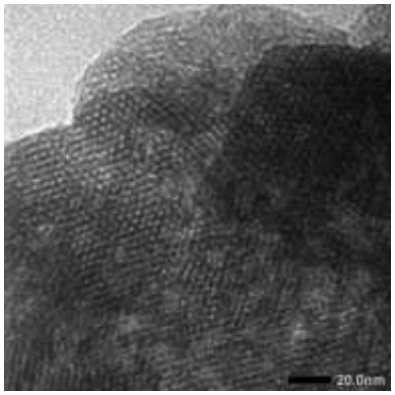

Fig. 2. TEM of Ni-MCM-41

3.1.3 N_2 Adsorption–Desorption Analysis

The textural properties of synthesized Ni-MCM-41 obtained from N_2 adsorption-desorption analysis are presented in Table 1, while the corresponding adsorption-desorption isotherm is shown in Fig. 3. The isotherm showed the typical behavior of mesoporous material, with capillary condensation occurring at relative pressure values associated with mesopore filling. The BET surface area of Ni-MCM-41 was 545.473 m²/g, with a total pore volume of 0.559 cm³/g and an average pore diameter of 2.786 nm. This pore diameter falls within the mesoporous range of 2–50 nm. The high surface area and mesoporous structure indicate that Ni-MCM-41 has good potential as a catalyst support because it can provide accessible surface sites and diffusion pathways for reactant molecules. Similar findings have been reported in studies on MCM-41-based materials characterized using BET and pore structure analysis [16], [19].

Table 1. Textural properties of Ni-MCM-41

Material	Surface Area (m^2/g)	Pore Volume (cm^3/g)	Pore Diameter (nm)
Ni-MCM-41	545.473	0.559	2.786

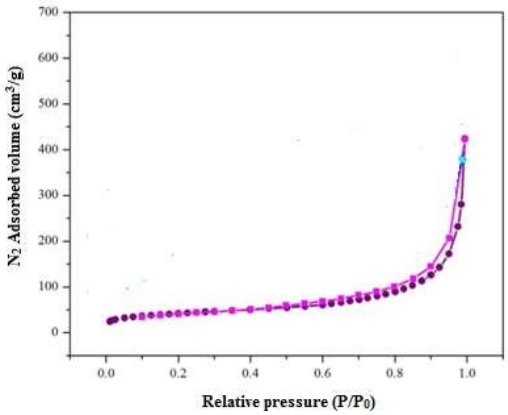

Fig. 3. N_2 Isotherm of Ni-MCM-41

3.2 Synthesis and Characterization of MnO_2/Ni-MCM-41

3.2.1 FTIR Analysis

The FTIR spectra of Ni-MCM-41 and MnO_2/Ni-MCM-41 are shown in Fig. 4, indicating the characteristic vibrations of the silica framework and the successful incorporation of MnO_2 species after impregnation and calcination. The spectra showed characteristic bands of the silica framework, including Si-O-Si bending and stretching vibrations. Peaks around 456 cm^{-1}, 796 cm^{-1}, and 1085 cm^{-1} can be assigned to the vibration modes of the Si-O-Si framework. The band around 957 cm^{-1} is associated with silanol groups and possible Si-O-Ni vibration, indicating nickel modification of the MCM-41 structure. A broad absorption band around 3500 cm^{-1} also indicates the presence of surface hydroxyl groups. These FTIR characteristics are consistent with previous studies on MCM-41 and metal-modified mesoporous silica materials [16], [18].

After impregnation with $MnSO_4$ and calcination, the MnO_2/Ni-MCM-41 catalyst showed an additional absorption band around 562 cm^{-1}, which can be attributed to Mn-O vibration. This result indicates that manganese oxide species were successfully introduced into the Ni-MCM-41 support. The presence of both silica framework vibrations and Mn-O vibration suggests that the impregnation process introduced MnO_2 while preserving the main mesoporous silica framework. Similar impregnation-based modifications have been reported in MCM-41-supported metal oxide catalysts, where metal species are deposited onto the surface or inside the pore channels of the mesoporous support [16], [18].

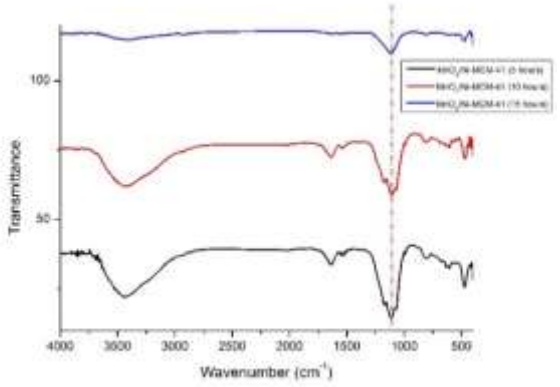

Fig. 4. FTIR MnO_2/Ni-MCM-41 variation of impregnation 5 h, 10 h, and 15 h

3.2.2 XRD Analysis

The XRD patterns of MnO_2/Ni-MCM-41 with different impregnation times are shown in Fig. 5. The characteristic low-angle peaks of MCM-41 were still present after MnO_2 incorporation. This result indicates that the ordered mesoporous structure was partially preserved after impregnation and calcination. The diffraction pattern also showed a broad peak around 2θ ≈ 25°, which may be associated with poorly crystalline manganese oxide species. Poorly crystalline Mn-based oxide catalysts are commonly reported in CO oxidation studies because manganese oxide species can form dispersed oxide domains depending on precursor type, calcination condition, and interaction with the support [20]–[23].

However, the specific assignment of this peak to birnessite-type δ-MnO_2 should be verified directly using the official ICDD/JCPDS database. Therefore, the safer interpretation is that the broad peak indicates the formation of dispersed or poorly crystalline manganese oxide species on the Ni-MCM-41 support. The 10 h impregnation sample showed more defined structural characteristics than the 5 h and 15 h samples. This result suggests that 10 h impregnation provided a better balance between MnO_2 deposition and preservation of the mesoporous framework.

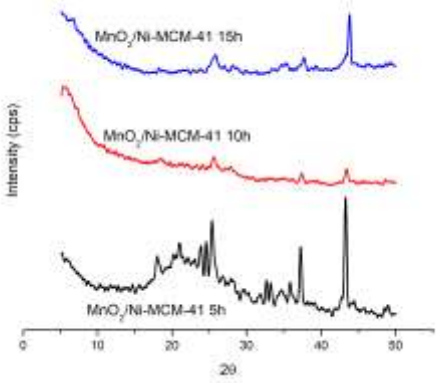

Fig. 5. Diffractogram pattern of MnO_2/Ni-MCM-41

3.2.3 N_2 Adsorption–Desorption Analysis

The surface area and pore structure characteristics of MnO_2/Ni-MCM-41 composites were evaluated using nitrogen adsorption–desorption isotherms, as summarized in Table 2. The surface area decreased from 357.234 m^2/g for the 5 h sample to 265.664 m^2/g for the 10 h sample and 220.047 m^2/g for the 15 h sample. The pore volume also decreased from 0.427 cm^3/g to 0.389 cm^3/g and 0.174 cm^3/g, respectively. This reduction indicates that MnO_2 species were deposited within or near the mesoporous channels, causing partial pore blockage. Similar behavior has been reported in metal-loaded MCM-41 systems, where metal incorporation can reduce surface area and pore volume due to the deposition of active species inside the pore channels or on the external surface [16], [18], [19].

Table 2. Textural properties of MnO_2/Ni-MCM-41 at different impregnation times

Material	Surface Area (m^2/g)	Pore Volume (cm^3/g)	Pore Diameter (nm)
MnO_2/Ni-MCM-41 (5 h)	357.234	0.427	2.975
MnO_2/Ni-MCM-41 (10 h)	265.664	0.389	3.653
MnO_2/Ni-MCM-41 (15 h)	220.047	0.174	5.087

The average pore diameter increased from 2.975 nm for the 5 h sample to 3.653 nm for the 10 h sample and 5.087 nm for the 15 h sample. This increase may indicate pore widening, partial wall reconstruction, or selective blockage of smaller pores after MnO_2 deposition. In Mn-based catalysts, structural and textural properties strongly influence catalytic performance because they affect active-site accessibility and oxygen mobility during CO oxidation [20], [23], [24]. The 10 h impregnation sample showed a balanced textural condition because it maintained sufficient surface area and pore volume while allowing MnO_2 species to be incorporated into the support.

3.3 Catalytic Activity for CO Oxidation

The catalytic activity test was conducted using exhaust gas from a four-stroke motorcycle under idle conditions. The test compared three conditions: without catalyst, MnO_2, and MnO_2/Ni-MCM-41 with different impregnation times. The decrease in CO concentration and the increase in CO_2 concentration indicate that CO oxidation occurred over the catalyst surface, as shown in Figs. 6 and 7. This result supports the role of MnO_2 as an active phase for CO oxidation. Manganese oxide catalysts are known to support CO oxidation because Mn species can provide redox-active sites and surface oxygen species involved in the oxidation process [8]–[10], [20], [21].

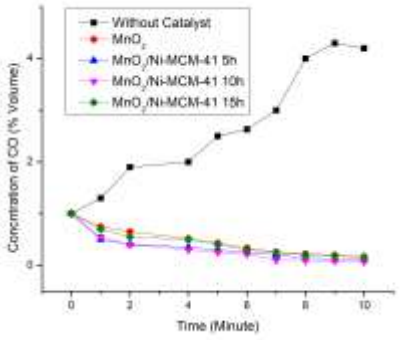

Fig. 6. Catalytic activity for CO removal

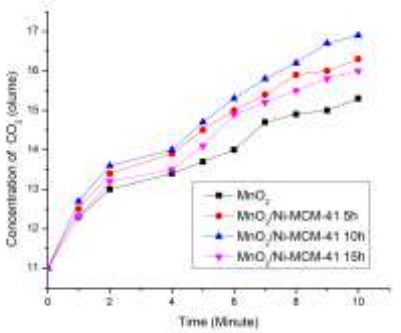

Fig. 7. Catalytic activities for CO_2 forming

The MnO_2/Ni-MCM-41 catalyst with 10 h impregnation showed the best catalytic performance among the tested samples. This result can be explained by the balance between active MnO_2 loading and preservation of the mesoporous structure. Shorter impregnation time may produce insufficient active sites, while longer impregnation time may cause excessive MnO_2 deposition, pore blockage, and lower surface accessibility. The 10 h sample likely provided better active-site dispersion, oxygen mobility, and gas diffusion pathways. These factors are important for CO oxidation because the reaction requires accessible active sites and efficient contact between CO, oxygen species, and the catalyst surface [20], [23], [24].

The catalytic behavior of MnO_2/Ni-MCM-41 can be associated with a redox mechanism. CO molecules are first adsorbed on the catalyst surface, then react with oxygen species from manganese oxide to form CO_2. Oxygen vacancies formed during the reaction can be replenished by oxygen from the exhaust gas. This pathway is consistent with the Mars-van Krevelen mechanism commonly discussed in CO oxidation over transition metal oxide catalysts [20], [21], [24]. In this system, Ni-MCM-41 acts as a support that improves MnO_2 dispersion and facilitates mass transfer through its mesoporous structure. The enhanced performance of the 10 h MnO_2/Ni-MCM-41 catalyst can therefore be attributed to the combined effect of MnO_2 redox activity, oxygen mobility, and Ni-MCM-41 structural support. Recent MnO_2-based catalyst studies also show that metal interaction, oxygen vacancies, and nanodispersed active sites can improve low-temperature CO oxidation performance [21], [25].

4. Conclusion

MnO_2/Ni-MCM-41 was successfully synthesized via hydrothermal method followed by wet impregnation and calcination. The Ni-MCM-41 exhibited a hexagonal mesostructure, indicating the successful incorporation of Ni into the MCM-41 framework. Among the prepared catalysts, MnO_2/Ni-MCM-41 with an impregnation time of 10 h showed the best structural and catalytic performance, as confirmed by the presence of characteristic peaks of MCM-41 and δ-MnO_2 in the XRD pattern. MnO_2 likely serves as the primary active phase, playing a crucial role in the CO oxidation process. Further investigations involving XPS, H_2-TPR, EDS mapping, oxygen mobility analysis, and long-term durability testing are necessary to fully elucidate the Mn–Ni synergistic interaction, oxygen vacancy concentration, and catalyst stability during prolonged catalytic oxidation. The optimal catalyst demonstrated a significant reduction in CO concentration, reaching up to 0.1 mg/L within 10 min of reaction, indicating its high efficiency for CO oxidation.

Acknowledgment

The authors gratefully acknowledge the financial support provided by the Ministry of Research, Technology, and Higher Education of the Republic of Indonesia through the *Program Kreativitas Mahasiswa – Penelitian Eksakta (PKM-PE) 2019*. The authors also express their appreciation to the Material Chemistry and Energy Laboratory, Institut Teknologi Sepuluh Nopember, for providing research facilities.

References

[1] Sukarno, I., Matsumoto, H., & Susanti, L. (2016). Transportation energy consumption and emissions: A view from city of Indonesia. *Future Cities and Environment, 2*, Article 6. https://doi.org/10.1186/s40984-016-0019-x

[2] Mahalana, A., Yang, L., Dallmann, T., Lestari, P., Maulana, K., & Kusuma, N. (2022). *Measurement of real-world motor vehicle emissions in Jakarta*. The Real Urban Emissions Initiative. https://trueinitiative.org/wp-content/uploads/2024/11/true-jakarta-report-en.pdf

[3] Hassani, A., & Hosseini, V. (2016). An assessment of gasoline motorcycle emissions performance and understanding their contribution to Tehran air pollution. *Transportation Research Part D: Transport and Environment, 47*, 1–12. https://doi.org/10.1016/j.trd.2016.05.003

[4] Mahesh, S., Ramadurai, G., & Shiva Nagendra, S. M. (2019). Real-world emissions of gaseous pollutants from motorcycles on Indian urban arterials. *Transportation Research Part D: Transport and Environment, 76*, 72–84. https://doi.org/10.1016/j.trd.2019.09.010

[5] Giechaskiel, B. (2020). Gaseous and particulate emissions of a Euro 4 motorcycle and effect of driving style and open or closed sampling configuration. *Sustainability, 12*(21), 9122. https://doi.org/10.3390/su12219122

[6] Rose, J. J., Wang, L., Xu, Q., McTiernan, C. F., Shiva, S., Tejero, J., & Gladwin, M. T. (2017). Carbon monoxide poisoning: Pathogenesis, management, and future directions of therapy. *American Journal of Respiratory and Critical Care Medicine, 195*(5), 596–606. https://doi.org/10.1164/rccm.201606-1275CI

[7] Eichhorn, L., Thudium, M., & Jüttner, B. (2018). The diagnosis and treatment of carbon monoxide poisoning. *Deutsches Ärzteblatt International, 115*(51–52), 863–870. https://doi.org/10.3238/arztebl.2018.0863

[8] Dey, S., Dhal, G. C., Mohan, D., & Prasad, R. (2018). Low-temperature complete oxidation of CO over various manganese oxide catalysts. *Atmospheric Pollution Research, 9*(4), 755–763. https://doi.org/10.1016/j.apr.2018.01.020

[9] Dey, S., & Mehta, N. S. (2020). Selection of manganese oxide catalysts for catalytic oxidation of carbon monoxide at ambient conditions. *Resources, Environment and Sustainability, 1*, 100003. https://doi.org/10.1016/j.resenv.2020.100003

[10] Dey, S., & Praveen Kumar, V. V. (2020). The performance of highly active manganese oxide catalysts for ambient conditions carbon monoxide oxidation. *Current Research in Green and Sustainable Chemistry, 3*, 100012. https://doi.org/10.1016/j.crgsc.2020.100012

[11] Martínez-Edo, G., Balmori, A., Pontón, I., Martí del Rio, A., & Sánchez-García, D. (2018). Functionalized ordered mesoporous silicas MCM-41: Synthesis and applications in catalysis. *Catalysts, 8*(12), 617. https://doi.org/10.3390/catal8120617

[12] Reato, P. T., Todero, A. S., de Oliveira Pereira, F., Dallago, R. M., Bernardo-Gusmão, K., & Mignoni, M. L. (2023). Mesoporous materials of the MCM type: Synthesis, application, use of ionic solids and functionalization with graphene: A review. *Silicon, 15*, 4345–4364. https://doi.org/10.1007/s12633-023-02344-3

[13] Oliveira, L. G., do Nascimento, C. T., Cazula, B. B., Tait, A., de Oliveira, C. J., Souza, G. E. Q., Gasparrini, L. J., Alencar, Á. O., Ritter, G., Jorge, N. N., & Alves, H. J. (2024). Nickel-stage addition in Si-MCM-41 synthesis for renewable hydrogen production. *Processes, 12*(9), 1836. https://doi.org/10.3390/pr12091836

[14] Uttamaprakrom, W., Reubroycharoen, P., Charoensiritanasin, P., Tatiyapantarak, J., Srifa, A., Koo-Amornpattana, W., Chaiwat, W., Sakdaronnarong, C., Sudoh, M., Watanabe, R., Fukuhara, C., & Ratchahat, S. (2021). Development of Ni-Ce/Al-MCM-41 catalysts prepared from natural kaolin for CO_2 methanation. *Journal of Environmental Chemical Engineering, 9*(5), 106150. https://doi.org/10.1016/j.jece.2021.106150

[15] Admi, Mardiah, R., & Arief, S. (2022). Sintesis dan karakterisasi Ni/MCM-41 dengan metode hidrotermal. *Jurnal Kimia Unand, 11*(1), 1–5. https://doi.org/10.25077/jku.11.1.1-5.2022

[16] Morais, L. A., Castro, F. L., Fernandes, G. J. T., Araujo, M. D. S., Farias, M. F., Guedes, A. P. M. A., Fernandes, V. J., Jr., & Araujo, A. S. (2023). Synthesis and characterization of MCM-41 nanomaterials containing titanium and application for catalytic oxidation of BTEX. *Catalysis Research, 3*(2), 017. https://doi.org/10.21926/cr.2302017

[17] Samriani, S., Zakir, M., Taba, P., La Nafie, N., & Indriani, I. (2022). Synthesis of MCM-41 silica mesoporous modified with Zn metal. *Jurnal Kimia Sains dan Aplikasi, 25*(8), 286–291. https://doi.org/10.14710/jksa.25.8.286-291

[18] Hachemaoui, M., Molina, C. B., Belver, C., Bedia, J., Mokhtar, A., Hamacha, R., & Boukoussa, B. (2021). Metal-loaded mesoporous MCM-41 for the catalytic wet peroxide oxidation (CWPO) of acetaminophen. *Catalysts, 11*(2), 219. https://doi.org/10.3390/catal11020219

[19] Tella, J. O., Ajanaku, K. O., Adekoya, J. A., Banerjee, R., Patra, C. R., Pavuluri, S., & Sreedhar, B. (2024). Physicochemical and textural properties of amino-functionalised

mesoporous silica nanomaterials from different silica sources. *Results in Chemistry, 7*, 101505. https://doi.org/10.1016/j.rechem.2024.101505

[20] Li, X., Ren, S., Chen, Z., Wang, M., Chen, L., Chen, H., & Yin, X. (2023). A review of Mn-based catalysts for abating NOx and CO in low-temperature flue gas: Performance and mechanisms. *Molecules, 28*(19), 6885. https://doi.org/10.3390/molecules28196885

[21] Gong, X., Xu, J., Zhang, T., Sun, Y., Fang, S., Li, N., Zhu, J., Wu, Z., Li, J., Gao, E., Wang, W., & Yao, S. (2023). DRIFTS-MS investigation of low-temperature CO oxidation on Cu-doped manganese oxide prepared using nitrate aerosol decomposition. *Molecules, 28*(8), 3511. https://doi.org/10.3390/molecules28083511

[22] Bulavchenko, O. A., Afonasenko, T. N., Osipov, A. R., Pochtar', A. A., Saraev, A. A., Vinokurov, Z. S., Gerasimov, E. Y., & Tsybulya, S. V. (2021). The formation of Mn-Ce oxide catalysts for CO oxidation by oxalate route: The role of manganese content. *Nanomaterials, 11*(4), 988. https://doi.org/10.3390/nano11040988

[23] Bulavchenko, O. A., Konovalova, V. P., Saraev, A. A., Kremneva, A. M., Rogov, V. A., Gerasimov, E. Y., & Afonasenko, T. N. (2023). The catalytic performance of CO oxidation over MnOx-ZrO_2 catalysts: The role of synthetic routes. *Catalysts, 13*(1), 57. https://doi.org/10.3390/catal13010057

[24] Zhao, N., Dong, F., Kang, Y., Wu, L., & Tang, Z. (2026). Research progress and future challenges of CO oxidation catalysts: Preparation, catalytic performance, reaction mechanism and anti-poisoning strategies. *Journal of Materials Chemistry A, 14*, 11083–11117. https://doi.org/10.1039/D5TA09749E

[25] Blinov, E. D., Kulchakovskaya, E. V., Sokovikov, N. A., Svetlichnyi, V. A., Kulinich, S. A., & Vodyankina, O. V. (2025). Unravelling the Cu and Ce effects in MnO_2-based catalysts for low-temperature CO oxidation. *Nanomaterials, 15*(3), 166. https://doi.org/10.3390/nano15030166